On-chip near-infrared spectroscopy of CO$_2$ using high resolution plasmonic filter array

Xinyuan Chong, Erwen Li, Kenneth Squire, and Alan X. Wang

School of Electrical Engineering and Computer Science, Oregon State University, Corvallis, Oregon 97331, USA

We report an ultra-compact, cost-effective on-chip near-infrared spectroscopy system for CO$_2$ sensing using narrow-band optical filter array based on plasmonic gratings with a waveguide layer. By varying the periodicity of the gratings, the transmission spectra of the filters can be continuously tuned to cover the 2.0 μm sensing window with high spectral resolution around 10 nm. Our experimental results show that the on-chip spectroscopy system can resolve the two symmetric vibrational bands of CO$_2$ at 2.0 μm wavelength, which proves its potential to replace the expensive commercial IR spectroscopy system for on-site gas sensing. *Published by AIP Publishing.*
[http://dx.doi.org/10.1063/1.4953261]

Carbon dioxide (CO$_2$) is the most important greenhouse gas and the major product of combustion. Detecting CO$_2$ is critical for many practical applications such as combustion control[1] and pollution monitoring.[2] Of all existing gas sensor technologies, infrared (IR) absorption is widely used as a simple and reliable technique for both detection and identification of hazardous and greenhouse gases. IR spectroscopy relies on the optical absorption of molecular vibration bands, which represent the signatures of various gas molecules. Generally, existing IR detection techniques can be divided into two categories: spectroscopy and non-dispersive techniques. Non-dispersive techniques, as the name implies, do not have wavelength dispersive component, such as grating. Therefore, it will not provide spectroscopy information about the sample. In contrast, due to the wavelength dispersive components, spectroscopy techniques are able to detect multiple samples simultaneous by the unique spectral feature of the sample. In contrast, spectroscopy system is much more complicated, which contains wavelength dispersive components. It allows the spectroscopy techniques to detect multiple samples simultaneous by the unique spectral feature of the sample. In the mid-infrared (MIR, 2.5–25 μm) region, both of these sensing techniques offer remarkably high sensitivity by probing the fundamental vibrational and rotational transitions of CO$_2$ molecules. In the near-infrared (NIR, 0.8–2.5 μm) region, the absorption comes from the overtones of the fundamental bands, and is usually two to three orders of magnitude lower than that of the MIR, which results in relatively low sensitivity. In addition, the absorption bands of various gases are close to each other or even partially overlapped in the NIR region, which makes it difficult for non-dispersive techniques. Therefore, NIR spectroscopy can provide unprecedented specificity and multiplex gas sensing capabilities compared with non-dispersive techniques.[3–6] However, existing IR spectroscopy systems such as Fourier transform infrared (FTIR) spectroscopy are bulky, expensive, and power-hungry table-top equipment that can only be used in the laboratory. Therefore, there is a strong need to develop miniaturized on-chip NIR spectroscopy for on-site or portable gas sensing. Particularly for CO$_2$ sensing, there

are two major absorption bands in the NIR region: 1.57 μm and 2.0 μm. Because of the matured optical telecommunication industry, optoelectronic devices at 1.57 μm window such as light sources, spectrometers, and photodiodes are cost-effective, miniaturized, and widely available. Unfortunately, the sensitivity at 1.57 μm is extremely low ($\sim$1.8 $\times$ 10^{-3} cm^{-1}), and it requires an ultra-long absorption path length that can only be provided by multi-pass gas cells[7,8] to achieve high sensitivity. On the other hand, 2.0 μm wavelength can provide 70$\times$ stronger absorption (0.135 cm^{-1}). Some recent work has been published on 2.0 μm CO$_2$ NIR spectroscopy due to the availability of the light sources.[6,9–11] Nevertheless, they utilize either expensive distributed-feedback (DFB) lasers or bulky FTIR spectrometers. Therefore, ultra-compact spectrometers[12,13] still remain a grand challenge and research focus.

In this paper, we develop a simple and cost-effective plasmonic narrow-band filter array on a single chip, covering the wavelength range from 1990 nm to 2040 nm. Plasmonic filters are actually based on the well-known phenomena called "extraordinary optical transmission" (EOT).[14–16] By exploiting plasmonic nanostructures, such as nanohole or nanoslit arrays, efficient conversion between photons and plasmons can be controlled at subwavelength scale, leading to very high optical transmission, which provides alternative solutions to traditional optical processes such as color filtering and spectral imaging.[17–23] Compared with existing plasmonic filters at visible and UV wavelength ranges, we focused on the design of NIR wavelength filter array with high spectral resolution. By measuring the transmitted power of each filter, the spectroscopy information can be extracted. Most of the reported plasmonic filters are used for color filters with relatively low resolution (>50 nm). Due to the compactness and low cost of this filter array, it can potentially replace the expensive and bulky FTIR spectroscopy systems for mobile NIR gas sensing.

The configuration of the plasmonic filter is shown in Figure 1(a), which consists of a gold (Au) thin film with periodic nano-slits on a quartz (n$_{sub}$ = 1.45) substrate. A layer of UV cured SU-8 (n$_{SU-8}$ = 1.57) photoresist covers the Au thin film, serving as a waveguide layer. Transverse magnetic (TM)
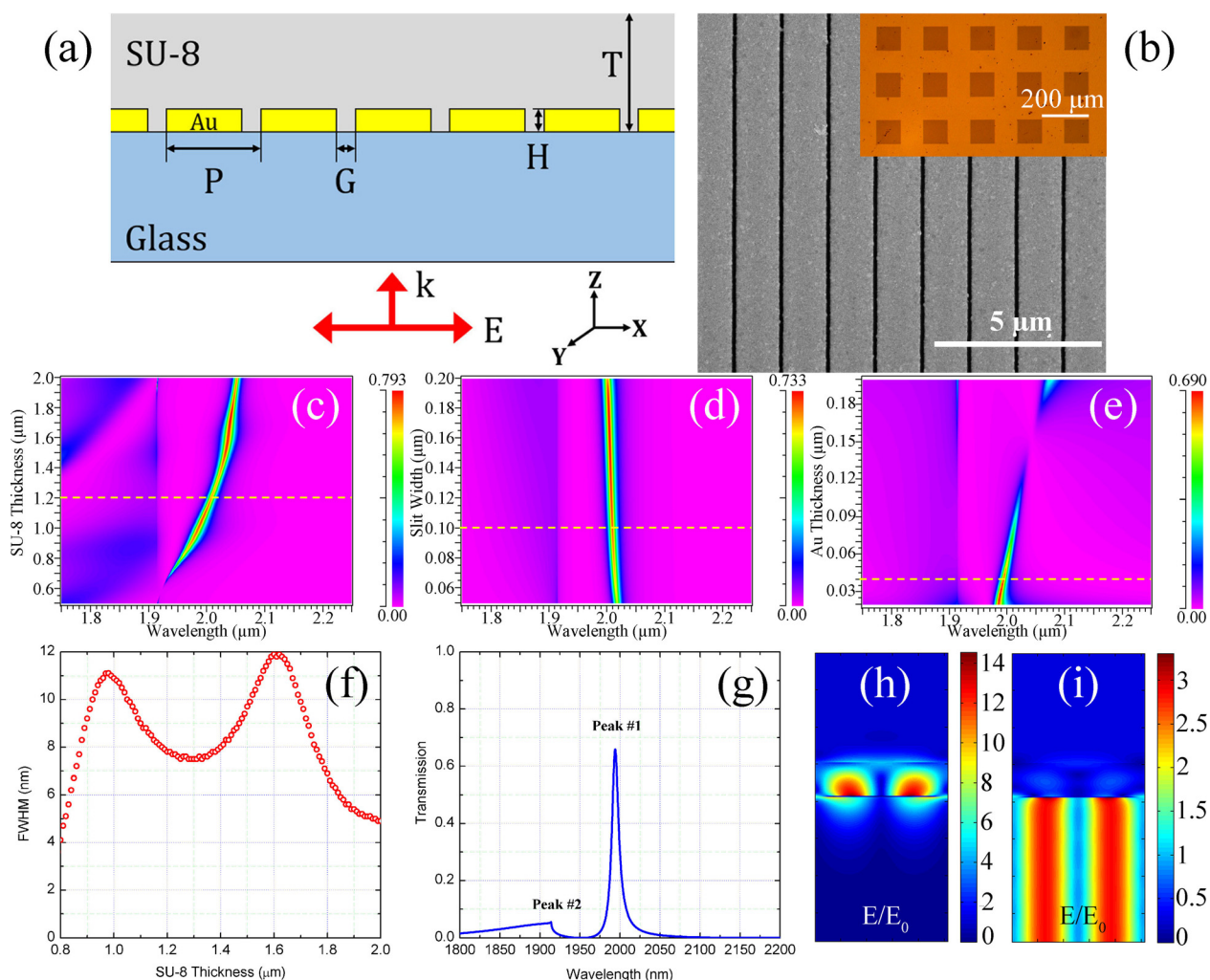
108, 221106-1

FIG. 1. (a) The configuration of the plasmonic filter and the polarization of the incident light. The design parameters include: P—periodicity of grating, G—slit width, H—Au film thickness, and T—SU-8 thickness. (b) Scanning electron microscope image of Au film with nano-slit. Inset is the optical image of the filter array. Transmission spectra of the plasmonic filter: (c) the effect of SU-8 thickness, (d) slit width and (e) Au film thickness. (f) The full width half maximum (FWHM) of the transmission spectrum as a function of SU-8 thickness. (g) An example of the transmission spectrum using the optimized parameters. (h) Hybrid electric field distribution of major peak and (i) side-band. The electric field amplitude is normalized to that of the incident light E_0. Dashed lines represent the design parameters used in the experiment.

polarized light will be launched from the substrate side and normally incident on the filters. By varying the period P of the nano-slit, the transmission peak can be continuously tuned. The periodicity P also slightly affects the peak transmission intensity. However, within our interested wavelength range (1.98–2.04 μm), the effect is minor. The scanning electron microscope (SEM) image of the Au film with nano-slit is shown in Figure 1(b). There are three parameters that affect the transmission spectrum: the slit width G, Au thin thickness H and SU-8 thickness T, which are scanned to achieve small full width half maximum (FWHM), high transmission amplitude and less side-bands effects based on rigorous coupled-wave analysis (RCWA). As shown in Figures 1(c)–1(e), the effects of the SU-8 thickness, slit width, and Au film thickness to the transmission spectrum are studied. It is found that the thickness of SU-8 plays the most important role. It not only influences the FWHM but also contributes to the transmission amplitude and side-bands. Thinner SU-8 layer may cause cut-off (discontinuity) of the waveguide mode, while thicker film will generate higher order waveguide modes and the coupling

between higher order waveguide modes and Rayleigh Anomaly (RA). RA is associated with light diffracted parallel to the grating surface, which is determined by dielectric constant of the substrate, surrounding medium and the grating pitch.[24] In our case, the RA happens on the substrate side. The FWHM of the spectrum as a function is shown in Figure 1(f). For the slit width, it only slightly affects the transmission amplitude and FWHM. Wider slit width will allow more light passing through, but the FWHM will also increase. For Au film thickness, thinner film shows larger transmission amplitude and larger FWHM. However, if the Au thickness is too thin, the overall noise level of the spectrum will increase. Besides, at certain thickness, the cavity resonance in the nano-slit and the surface plasmon polariton on Au surface will have deconstructive interference, which will cause the discontinuity shown in the Figure 1(e).[25–29] Finally, the three parameters are chosen to be G = 100 nm, H = 40 nm and T = 1.2 μm (dashed line). Although the FWHM at T = 1.2 μm is slightly larger than that at T = 1.3 μm (<1 nm), the side-band effect is less at T = 1.2 μm. An example of the transmission spectrum using

the chosen values is shown in Figure 1(g). There are two transmission peaks on the spectrum, representing two different modes. The major peak (#1) at ~2.0 μm represents the coupling mode between surface plasmon at SU-8/Au interface and the narrow-band waveguide mode supported by the SU-8 waveguide layer. The side band (#2) at ~1.91 μm is due to the Rayleigh Anomaly in the glass substrate.[30–34] The normalized electric field amplitude distribution of the two modes is shown in Figures 1(h) and 1(i).

The filters are fabricated by focused ion beam (FIB) etching followed spin-coating SU-8. As shown in the inset of Figure 1(b), eventually, there are 15 filters in total. The size of each filter is $100\,\mu$m $\times\,100\,\mu$m and the total area of the filter array is less than $1\,$mm^2. The transmission spectrum of each filter is calibrated by an optical spectrum analyzer (OSA). Figure 2(a) and 2(b) show both the numerically simulated and experimentally obtained transmission spectrum of each filter. Comparing the two sets of spectra, two discrepancies between simulation and experiment: (1) the amplitude of the transmission spectra in the
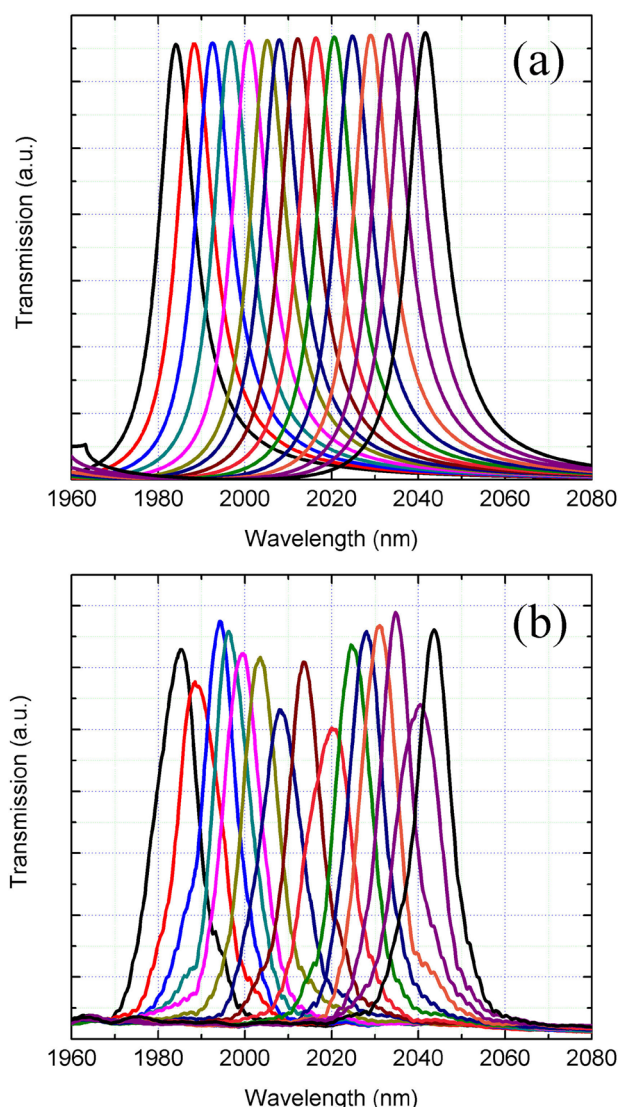
experiment fluctuate from filter to filter. It is mainly due to the non-uniformity of the SU-8 film. (2) The FWHM of the experimental obtained spectrum (10–12 nm) is slightly larger than the simulation (7–9 nm), which is induced by the variation of both the nano-slit width and imperfection of the thermal evaporated Au thin film.

To demonstrate the capability of the filter array for gas sensing application, a spectroscopy system using the filter array is built as shown in Figure 3(a). The collimated light from a supercontinuum light source (NKT Photonics, 400 nm–2400 nm, 10 kHz) first passes through a linear polarizer (Thorlabs, Inc., LPNIR050) to obtain TM light. A band-pass filter (Thorlabs, Inc., FB2000-500) is used to shrink the wavelength range to 1750 nm to 2250 nm to avoid undesired side bands. Due to the large beam diameter of the light source comparing to the filter, a simple beam expander is reversely used to shrink the beam size to obtain high power density. The shrunk light passes then through a 10 cm quartz gas cell. The light transmitted through the filter is collected by a multi-mode fiber (MMF) and delivered to a PbS photodetector (Thorlabs, Inc., PDA30G). Since the photodetector is AC coupled, a chopper is applied to convert the CW light to pulsed light. Finally, the electric signal from the photodetector is sent to an oscilloscope. It should be noted that, although in the experiment setup, an MMF is used to collect the light transmitted through the filters, it can be replaced by a charge-coupled device (CCD) or photodetector array placed directly behind the filter array. In this way, signals from each filter can be collected simultaneously, which allows high speed detection. Moreover, without MMF, there will be no alignment or coupling stability issue, which may induce extra noise.

The transmitted power of each filter through a gas cell filled with CO_2 is recorded. The same measurement for Ar is taken as the reference. Since Ar does not absorb any light around 2.0 μm, the subtraction between the transmitted power of CO_2 and Ar will be the NIR absorption due to CO_2. The absorption spectrum of CO_2 obtained by this system (black line with red square) is shown in Figure 3(b). As a comparison, the experimental data from conventional FTIR (blue lines) is also shown. It is clearly seen that the two vibration bands are resolved, which matches the experimental results using conventional FTIR. The slight variation (~1 nm) between these two experimental methods can possibly come from fabrication variation and the limited resolution of the filter array.

To evaluate the capability of current system, the noise of the signal is studied. After chopping, the signal received by the oscilloscope is a square wave, as shown in Figure 3(c). The voltage difference between the top and bottom flat regions will represent the actual voltage associated with transmitted light. The top region represents the signal when light is blocked by the chopper, and the bottom region represents the signal when the light is unblocked. It is noticed that, in the bottom region, there is a regular low frequency (~10 kHz) variation in addition to the high frequency noise. This variation is caused by the frequency of the pulsed light source. Such regular variation can be easily filtered out, as shown in Figure 3(d). The noises of the top and bottom flat regions are represented by the standard deviation σ_t and σ_b,
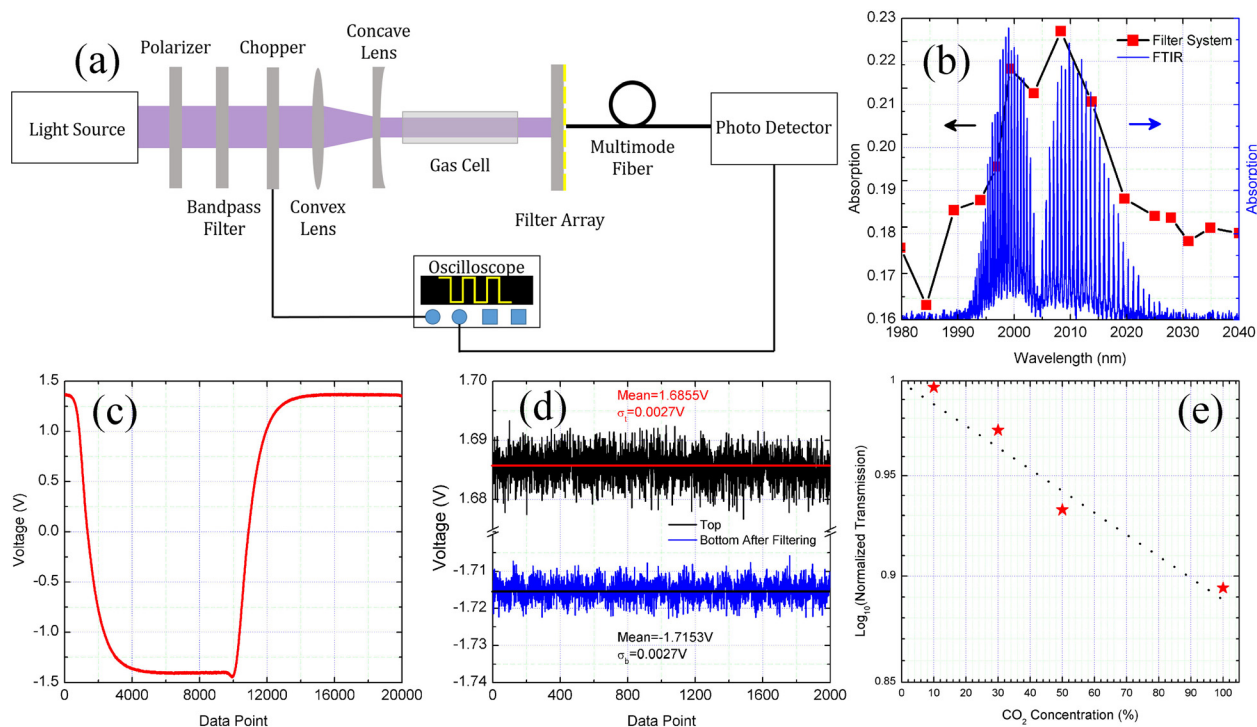

FIG. 2. (a) Numerically simulated and (b) experimentally obtained transmission spectrum of each filter. G = 100 nm, H = 40 nm, and T = 1.2 μm, and the period varies from 1313 nm to 1354 nm with 4 nm step.

FIG. 3. (a) Experiment setup for CO_2 sensing; (b) experimental absorption spectrum of CO_2; (c) signal received by oscilloscope; (d) noise level of the top and bottom flat region after filtering; and (e) normalized transmission as a function of CO_2 concentration.

both of which are 0.0027 V. When there is absorption caused by CO_2, the bottom trace will move up. In order to distinguish the signal change due to the CO_2 absorption, the voltage change has to be at least $3\sigma_t + 3\sigma_b$.[35,36] Therefore, the minimum detection is defined to be $\sigma = 3\sigma_t + 3\sigma_b$. The voltage change at the peak absorption is 0.7537 V, which is about 46.52 times of σ. We measured the normalized transmission as a function of different CO_2 concentration, which is shown in Figure 3(e). A good linearity is observed, which matches the law of Beer-Lambert absorption. Here, we also define the sensitivity to be *minimum detectable CO_2 concentration × optical absorption length*. Therefore, for our current system, the sensitivity is about 214,957 ppm·cm. Webber *et al.* reported 144 000 ppm cm (Ref. 37) sensitivity for vent gas in a bioreactor and 5000 ppm cm (Ref. 11) for combustion gas using distributed feedback laser. It should be noted that as the noise level is relatively constant, the voltage change due to the CO_2 absorption is proportional to the intensity of the input light. Higher input light intensity will achieve lower detection limit. Therefore, the sensitivity of our on-chip NIR spectroscopy system can be improved by increasing the input light intensity or using a more stable light source. A lock-in amplifier to detect only the chopping frequency can also improve the signal-to-noise ratio and hence improve the detection limit.

In summary, we have designed and experimentally demonstrated an NIR on-chip spectroscopy system for CO_2 by an array of narrow-band plasmonic filters with 10–12 nm spectral resolution. The two vibrational bands of CO_2 are resolved, which matches the theoretical data from HITRAN database. By evaluating the noise level of the system, the sensitivity of current system is estimated to be 214 957 ppm cm. The sensitivity can be further improved by suppressing

the noise using lock-in amplifiers. Due to the advantage of compactness, low-cost, and easy-to-fabricate, this plasmonic filter array shows great potentials to replace the expensive and bulky FTIR spectroscopy system for mobile NIR gas sensing.

[1]A. Sanchez, E. Eddings, and F. Mondragon, Energy Fuel **24**, 4849 (2010).
[2]A. E. Andrews, J. D. Kofler, M. E. Trudeau, J. C. Williams, D. H. Neff, K. A. Masarie, D. Y. Chao, D. R. Kitzis, P. C. Novelli, C. L. Zhao, E. J. Dlugokencky, P. M. Lang, M. J. Crotwell, M. L. Fischer, M. J. Parker, J. T. Lee, D. D. Baumann, A. R. Desai, C. O. Stanier, S. F. J. De Wekker, D. E. Wolfe, J. W. Munger, and P. P. Tans, Atmos. Meas. Tech. **7**(2), 647 (2014).
[3]X. Y. Chong, K. J. Kim, P. R. Ohodnicki, E. W. Li, C. H. Chang, and A. X. Wang, IEEE Sens. J. **15**(9), 5327 (2015).
[4]V. Weldon, J. Ogorman, P. Phelan, J. Hegarty, and T. Tanbunek, Sens. Actuator, B **29**(1–3), 101 (1995).
[5]V. Weldon, J. Ogorman, P. Phelan, and T. Tanbunek, Opt. Eng. **33**(12), 3867 (1994).
[6]P. Werle, R. Mucke, F. D'Amato, and T. Lancia, Appl. Phys. B **67**(3), 307 (1998).
[7]D. Masiyano, J. Hodgkinson, and R. P. Tatam, Appl. Phys. B **100**(2), 303 (2010).
[8]S. Tranchart, I. H. Bachir, and J. L. Destombes, Appl. Opt. **35**(36), 7070 (1996).
[9]R. M. Mihalcea, M. E. Webber, D. S. Baer, R. K. Hanson, G. S. Feller, and W. B. Chapman, Appl. Phys. B **67**(3), 283 (1998).
[10]L. Sandstrom, S. Backstrom, H. Ahlberg, S. Hojer, and A. G. Larsson, Infrared Phys. Technol. **39**(2), 69 (1998).
[11]M. E. Webber, S. Kim, S. T. Sanders, D. S. Baer, R. K. Hanson, and Y. Ikeda, Appl. Opt. **40**(6), 821 (2001).

[12]H. Guo and J. P. Guo, Opt. Lett. **40**(2), 249 (2015).

[13]Y. Zou, S. Chakravarty, P. Wray, and R. T. Chen, Sens. Actuator, B **221**, 1094 (2015).

[14]T. W. Ebbesen, H. J. Lezec, H. F. Ghaemi, T. Thio, and P. A. Wolff, Nature **391**(6668), 667 (1998).

[15]H. T. Liu and P. Lalanne, Nature **452**(7188), 728 (2008).

[16]L. Martin-Moreno, F. J. Garcia-Vidal, H. J. Lezec, K. M. Pellerin, T. Thio, J. B. Pendry, and T. W. Ebbesen, Phys. Rev. Lett. **86**(6), 1114 (2001).

[17]Y. S. Do, J. H. Park, B. Y. Hwang, S. M. Lee, B. K. Ju, and K. C. Choi, Adv. Opt. Mater. **1**(2), 133 (2013).

[18]X. L. Hu, L. B. Sun, B. Shi, M. Ye, Y. Xu, L. S. Wang, J. Zhao, X. L. Li, Y. Q. Wu, S. M. Yang, R. Z. Tai, H. J. Fecht, J. Z. Jiang, and D. X. Zhang, J. Appl. Phys. **115**(11), 113104 (2014).

[19]A. F. Kaplan, T. Xu, Y. K. Wu, and L. J. Guo, J. Vac. Sci. Technol., B **28**(6), C6060 (2010).

[20]H. S. Lee, Y. T. Yoon, S. S. Lee, S. H. Kim, and K. D. Lee, Opt. Express **15**(23), 15457 (2007).

[21]T. Xu, Y. K. Wu, X. G. Luo, and L. J. Guo, Nat. Commun. **1**, 59 (2010).

[22]F. Ye, M. J. Burns, and M. J. Naughton, Sci. Rep. **4**, 7267 (2014).

[23]S. Yokogawa, S. P. Burgos, and H. A. Atwater, Nano Lett. **12**(8), 4349 (2012).

[24]H. Gao, J. M. McMahon, M. H. Lee, J. Henzie, S. K. Gray, G. C. Schatz, and T. W. Odom, Opt. Express **17**(4), 2334 (2009).

[25]K. L. Lee, J. B. Huang, J. W. Chang, S. H. Wu, and P. K. Wei, Sci. Rep. **5**, 8547 (2015).

[26]G. D'Aguanno, N. Mattiucci, M. J. Bloemer, D. de Ceglia, M. A. Vincenti, and A. Alu, J. Opt. Soc. Am. B **28**(2), 253 (2011).

[27]D. de Ceglia, M. A. Vincenti, M. Scalora, N. Akozbek, and M. J. Bloemer, AIP Adv. **1**(3), 032151 (2011).

[28]Y. Ding and R. Magnusson, Opt. Express **12**(23), 5661 (2004).

[29]H. Lochbihler and R. A. Depine, Appl. Opt. **51**(11), 1729 (2012).

[30]K. Y. Kim, X. Y. Chong, F. H. Ren, and A. X. Wang, Opt. Lett. **40**(22), 5339 (2015).

[31]F. F. Liu and X. P. Zhang, Biosens. Bioelectron. **68**, 719 (2015).

[32]D. B. Mazulquim, K. J. Lee, J. W. Yoon, L. V. Muniz, B. H. Borges, L. G. Neto, and R. Magnusson, Opt. Express **22**(25), 30843 (2014).

[33]A. T. M. A. Rahman, P. Majewski, and K. Vasilev, Opt. Lett. **37**(10), 1742 (2012).

[34]F. H. Ren, K. Y. Kim, X. Y. Chong, and A. X. Wang, Opt. Express **23**(22), 28868 (2015).

[35]J. D. Driskell, K. M. Kwarta, R. J. Lipert, M. D. Porter, J. D. Neill, and J. F. Ridpath, Anal. Chem. **77**(19), 6147 (2005).

[36]J. Yang, L. Zhen, F. Ren, J. Campbell, G. L. Rorer, and A. X. Wang, J. Biophotonics **8**(8), 659 (2015).

[37]M. E. Webber, R. Claps, F. V. Englich, F. K. Tittel, J. B. Jeffries, and R. K. Hanson, Appl. Opt. **40**(24), 4395 (2001).